27 May 2021
Michael C. McMahon
University of Minnesota
2003 Upper Buford Circle
Saint Paul, MN 55108
(651) 500-6370
mcmah231@d.umn.edu

RH: McMahon et al. · UAS for Deer Density Estimation

Comparing unmanned aerial systems to conventional methodology for surveying a wild white-tailed deer population

MICHAEL C. MCMAHON,[1] *Department of Fisheries, Wildlife, and Conservation Biology, University of Minnesota, 2003 Upper Buford Circle, Suite 135, Saint Paul, MN, 55108, USA*

MARK A. DITMER, *Department of Fisheries, Wildlife, and Conservation Biology, University of Minnesota, 2003 Upper Buford Circle, Suite 135, Saint Paul, MN, 55108, USA*

JAMES D. FORESTER, *Department of Fisheries, Wildlife, and Conservation Biology, University of Minnesota, 2003 Upper Buford Circle, Suite 135, Saint Paul, MN, 55108, USA*

[1] *Email: mcmah231@d.umn.edu*

Table of contents short summary

Ungulate populations are highly dynamic and require efficient survey methodology to inform management efforts. This study aimed to assess the efficacy of thermal sensor-equipped unmanned aerial systems (UAS) for estimating white-tailed deer densities, and found that UAS-based deer density estimates were comparable to conventional fecal pellet-group count-based density estimates. We find that UAS surveys offer an effective and temporally sensitive method for estimating wild ungulate densities.

Abstract

Context

Ungulate populations are subject to fluctuations caused by extrinsic factors and require efficient and frequent surveying to monitor population sizes and demographics. Unmanned aerial systems (UAS) have become increasingly popular for ungulate research; however, little is understood about how this novel technology compares to conventional methodologies for surveying wild populations.

Aims

We examined the feasibility of using a fixed-wing UAS equipped with a thermal infrared sensor for estimating the population density of wild white-tailed deer (*Odocoileus virginianus*) at the Cedar Creek Ecosystem Science Reserve (CCESR), Minnesota, USA. We compared UAS density estimates to those derived from fecal pellet-group counts.

Methods

We conducted UAS thermal survey flights from March to April of 2018 and January to March of 2019. Fecal pellet-group counts were conducted from April to May in 2018 and 2019. We modeled deer counts and detection probabilities and used these results to calculate point estimates and bootstrapped prediction intervals for deer density from UAS and pellet-group count data. We compared results of each survey approach to evaluate the relative efficacy of these two methodologies.

Key Results

Our best-fitting model of certain deer detections derived from our UAS-collected thermal imagery produced deer density estimates ($\bar{X}$ = 9.40, 95% prediction interval = 4.32–17.84 deer/km^2) that overlapped with the pellet-group count model when using our mean pellet deposition rate assumption ($\bar{X}$ = 7.01, 95% prediction interval = 4.14–11.29 deer/km^2). Estimates from our top UAS model using both certain and potential deer detections resulted in a mean density of 13.77 deer/km^2 (95% prediction interval = 6.64–24.35 deer/km^2); similar to our pellet-group count model that used a lower rate of pellet deposition ($\bar{X}$ = 10.95, 95% prediction interval = 6.46–17.65 deer/km^2). The mean point estimates from our top UAS model predicted a range of 136.68–273.81 deer, and abundance point estimates using our pellet-group data ranged from 112.79–239.67 deer throughout CCESR.

Conclusions

Overall, UAS yielded similar results to pellet-group counts for estimating population densities of wild ungulates; however, UAS surveys were more efficient and temporally sensitive.

Implications

We demonstrated how UAS could be applied for regularly monitoring changes in population density. We encourage researchers and managers to consider the merits of UAS and how they could be used to enhance the efficiency of wildlife surveying.

Introduction

The ability to collect data on population size and demographic vital rates frequently, accurately, and efficiently is critically important for monitoring wildlife populations undergoing rapid changes. Numerous ungulate populations throughout North America are in flux as a result of hunting pressure (Bonenfant et al. 2009), climatic and land use changes (Plante et al. 2018), disease (Edmunds et al. 2016), and changes to biological communities (Mech et al. 2018). White-tailed deer (*Odocoileus virginianus),* have adapted to and exploited various anthropogenic landscape and climatic changes resulting in a vast expansion of their geographic ranges and population densities (Dawe and Boutin 2016). Measuring the changes in deer populations is important to inform management actions intended to reduce ecological impacts associated with overgrazing (Mysterud 2006) and inter- and intraspecific disease transmission (Jennelle et al. 2014; Ditmer et al. 2020).

The recent rise in the use of unmanned aerial systems (UAS) for surveying wildlife populations is an especially attractive tool for monitoring dynamic populations because UAS offers a cheaper, safer, and more flexible alternative to conventional aircraft (Sasse 2003; Watts et al. 2010). Hourly operating costs may be reduced by as much as 82% with UAS, as compared to conventional aircraft (Vermeulen et al. 2013) and the logistics and regulations regarding their usage continue to diminish (Werden et al. 2015), especially when compared to manned aircraft flights (Linchant et al. 2015). Importantly, UAS may also increase survey accuracy as compared to traditional ground-based wildlife surveys (Chabot and Bird 2012). Hodgson et al. (2018) demonstrated that UAS data were on average 43% to 96% more accurate than replicated ground-based counts of seabirds within their colonies. When operators follow principles to reduce disturbance to wildlife (Hodgson and Koh 2016), unmanned aerial systems can minimise animal disturbance by removing the need to approach animals on foot (Krause et al. 2017), reducing the time humans spend in close proximity to study species (Weissensteiner et al. 2015), and by creating less noise than conventional aircraft (Bennitt et al. 2019).

UAS equipped with forward looking infrared (FLIR) sensors are a promising option for monitoring fluctuations in population size because wildlife surveys using UAS can be repeated frequently (Allan et al. 2018), assuming proper flight conditions, and can reduce operational costs (Elsey and Trosclair 2016) while improving survey accuracy (Lethbridge et al. 2019). Thermal sensors capture thermal radiation (i.e., body heat from animals), and thus increase the detection probability of warm-bodied animals, even at night or with partial obscuration from vegetation (Gill et al. 1997; Mulero-Pázmány et al. 2014; Montague et al. 2017). Aircraft-mounted thermal sensors improved detection of white-tailed deer relative to traditional ground-based spotlight surveys (Naugle et al. 1996). Due to the reduction in size and cost of both FLIR sensors and UAS, many researchers and managers are deploying them for ungulate research and population monitoring (Israel 2011; Lhoest et al. 2015; Chrétien et al. 2016; Witczuk et al. 2018; Beaver et al. 2020; McMahon et al. 2021).

Numerous technologies and methods, such as UAS-based approaches, are available for surveying critical population parameters; however, determining which ones provide the best balance of economic and time constraints on wildlife professionals is a constant challenge. Additionally, new methods and technologies may be resisted by agencies because of potential differences with historical baseline estimates; thus, assessing how new approaches compare to previously well-established methods is an active and important process for improving population monitoring. Ireland et al. (2019) found that UAS thermal surveys had greater spatial coverage and increased operational feasibility relative to camera trap surveys for detecting white-tailed deer at night. However, it is also important to understand how estimates from new methodologies compare to established, ‘low-tech’ methods, and to detail the tradeoffs in the costs, efforts, and learning curves among them. For example, Preston et al. (2021) compared the efficacy of UAS surveys to traditional spotlight surveys for deer, and found that spotlight approaches were underestimating deer densities.

Here, we compare population density estimates derived from a UAS with a mounted FLIR sensor to estimates based on fecal (pellet-group) surveys, a method frequently used to estimate the density of ungulate populations (Bennett et al. 1940; Eberhardt and Van Etten 1956). Pellet-group counts have been used for decades, and are still in use today (Gable et al. 2017), because of their cost effectiveness and ease of implementation. A major drawback of the approach is the requirement to estimate deer defecation and pellet decay rates, which can be difficult to obtain due to seasonal variation in diet and environmental conditions (Wallmo et al. 1962; Rogers 1987).

Our objectives were to: 1) examine the feasibility of using a fixed-wing UAS for detecting wild white-tailed deer (hereafter referred to as deer) in a forest-prairie interface, 2) determine deer population density from counts of deer in FLIR imagery, and 3) compare deer density estimates from UAS-gathered data to deer density estimates from pellet-group counts. We aim to provide information to wildlife professionals about whether UAS technology provides a significant advantage over cheaper and simpler conventional methodology, and how wildlife managers can most efficiently employ UAS technology to achieve research and management goals.

Study area

Surveys were conducted at the Cedar Creek Ecosystem Science Reserve (CCESR); located ~50 km north of Saint Paul, Minnesota, USA, near Bethel, Minnesota, in Anoka and Isanti counties (Fig. 1). This is a 2,200 ha experimental ecological reserve that the University of Minnesota operates in cooperation with the Minnesota Academy of Science (Cedar Creek Ecosystem Science Reserve 2019). Elevation at the site was consistent and ranged between 270 m to 295 m above sea level. Mean monthly temperatures at CCESR during our study period (March and April of 2018 and January to March of 2019) ranged between -13.11 °C to 0.44 °C, mean minimum temperatures were between -18.72 °C to -6.17 °C, and mean maximum temperatures ranged between -8.0 °C to 7.11 °C. Mean monthly precipitation ranged from 0.91 cm to 5.92 cm in rain and snow water equivalent (SWE). These weather data were collected by the Andover National Weather Service Reporting Station, ~ 19 km southwest of our study site (MNDNR 2019).

The CCESR property was located within the meeting point of western prairie ecosystems, northern hardwood forests, and eastern deciduous forests (Cedar Creek Ecosystem Science Reserve 2019). Land-cover types at CCESR included deciduous forest, conifer forest, forested wetland, emergent wetland, agriculture, grassland, developed areas, and open water (MN Land Cover Classification, 2013). Common wildlife species included white-tailed deer, coyote (*Canis latrans*), black bear (*Ursus americanus*), and wild turkey (*Meleagris gallopavo*), as well as various mesomammals.

Methods

UAS surveys

We conducted UAS thermal surveys across the CCESR property from March to April of 2018 and from January to March of 2019. We used a Sentera PHX Pro fixed-wing UAS equipped with a FLIR Vue Pro 640 (640 x 512 pixel resolution, 32° FOV, 19 mm lens, 30 Hz) (FLIR Systems Inc., Wilsonville, OR, USA) thermal sensor to detect white-tailed deer. We selected a fixed-wing UAS in favor of a multi-copter for increased flight endurance (Jiménez López and Mulero-Pázmány 2019) and reduced noise levels (M. McMahon, University of Minnesota, personal observation) to minimise wildlife disturbance. Survey plot locations were selected based on the availability of landing sites and our ability to maintain visual line of sight with the PHX. We identified landing zones across the CCESR property by intersecting areas of the highest relative elevation (Gesch et al. 2002) with areas of open and dry habitat types (NLCD 2011) using program R (R Core Team 2019). Launching from areas of higher relative elevation allowed us to maintain visual line of sight with the UAS during its course of flight (Federal Aviation Regulation 107.31). We considered open and dry areas of at least 335 m long and 30 m wide, depending on wind conditions, to be safe landing areas for the PHX. Flight survey plots were expanded from the landing zones to encompass as much land area as possible, with plot size limited by battery endurance of the PHX and the distance with which we could maintain un-aided visual contact. We originally identified nine survey plots with appropriate launch and landing zones; however, one plot was later removed due to our inability to safely land the UAS at that site. Our resulting eight survey plots ranged in size from 46.29 ha to 119.82 ha and encompassed 30.69% of the CCESR property in total (Fig. 1).

We pre-programmed the PHX to fly parallel transects at 121 m above ground level (AGL) over each survey plot using the laptop-based Sentera Ground Control program. We flew each plot at least twice per survey season, for a grand total of 35 survey flights, at various times of day from morning until evening. Parallel transects were used for efficiency and to minimise wildlife disturbance (Mulero-Pázmány et al. 2017), and we did not observe any behavioral reactions during the course of our study. The onboard thermal sensor was automatically triggered by the PHX's flight computer to achieve the pre-programmed image overlap. Thermal imagery was captured as still photos with 70 to 80% front overlap and 30% side overlap. Each image covered an average ground area of 3,948 m^2 (approximately 60 x 70 m ground distance). Images were geo-referenced from the PHX's GPS system and included data on altitude, speed, and bank angle of the UAS at the time of image capture. Imagery was saved on a mini SD card onboard the UAS, and was transferred post flight to an external hard drive and cloud-based storage system for post-processing.

UAS data analysis

We removed any imagery that was captured with UAS bank angles (amount of side-to-side roll) of >10° because imagery captured at greater angles of bank (e.g., during turn-arounds when the UAS was realigning to start new transects) would show inconsistent ground areas depending on bank angle, and would likely include space outside of our defined survey plots. We considered any bank angles of <10° to be products of ordinary wind turbulence during flight, based on observing the flight characteristics of the PHX and the distribution of bank angles in our data. We subsampled our thermal imagery for each plot by randomly selecting starting images and successively keeping any image with a centroid that was ≥ 80 m apart from any previously retained image's centroid, using program R. This process yielded a subsample of thermal imagery with a ground distance of 10 m to 24 m between the edges of thermal images to be analysed. This ensured that we did not analyse overlapping imagery, potentially recounting individual deer, and reduced the workload of reviewing the ~ 22,600 total thermal images collected.

We manually reviewed the subsampled imagery from each plot and recorded counts of deer observations that we classified as either 'certain' or 'potential' detections. Certain detections were recorded when we had no doubt that a deer was in the image based on the shape, size, and relative brightness of the thermal heat signature. Potential detections were less certain detections that may have only met some, but not all of our shape, size, and brightness search criteria. Deer were distinguished from other wildlife by relative size and shape, as they were the only animal of their size present (e.g., bears were in dens, and wolves are rarely found in the study area). Coyotes, which were present in the study area, could potentially be misidentified as deer but are generally smaller and less common than deer. Detection of deer fawns was not a factor since UAS surveys were flown prior to parturition, and young from the previous year would have been of sufficient size to meet the criteria used to detect adult deer. Prior to the start of the study, we recorded thermal imagery from a captive deer farm with a known number of deer. We used the imagery from the deer farm for training observers prior to reviewing field data. Imagery of the captive deer was taken with the same FLIR sensor at varying altitudes, angles, and amounts of vegetative cover to provide examples of how deer might appear in thermal imagery.

UAS deer density modeling

We modeled deer counts (i.e., the number of deer observed in a thermal image) using the glmmTMB package (Brooks et al. 2017) in program R because it allowed for the inclusion of zero-inflated models and random effects. This approach also allows for different model structures in the zero inflation and conditional components. Assumptions associated with zero-inflated distributions are similar to general abundance modeling and include; 1) a closed population, 2) independent individuals with equal availability for capture, and 3) applying the correct distribution given the presence of overdispersion in the data (Wenger and Freeman 2008). We believed that these assumptions were met relatively well. Although deer hunting occurs outside of the property boundaries, CCESR is closed to most public hunting, which is a leading cause of adult and fawn mortality (Brinkman et al. 2004). Wolves were not likely in the study area, and coyotes generally prey on fawns (Grovenburg et al. 2011), which would not have greatly impacted population demographics during our late winter to early spring study period. Furthermore, Rhoads et al. (2010) reported that female deer occupied an average seasonally-dependent home range of 21.2 ha for the 50% utilization distribution in an exurban population, which is a smaller area than our smallest UAS plot of 46.29 ha. Sub-sampling thermal imagery ensured independence among individuals by removing the potential to count the same deer more than once. Individual deer were relatively equally available to be detected using thermal imaging technology, and there was minimal conifer cover in the study area which could otherwise decrease detection probability (Dunn et al. 2002). We tested for overdispersion in the data, and appropriately applied zero-inflated negative-binomial models to account for the high number of zeros present in our data.

We included in our models the variables of sky cover (0 = clear sky, 1 = overcast sky) and the proportions of habitat cover type as possible fixed effects; a maximum of one cover type proportion was included per model component (i.e., each of the two component models could have at most sky cover and one land-cover proportion as a fixed effect). We used sky cover instead of ambient temperature because sky cover was previously shown to improve models of moose (*Alces alces*) detection over ambient temperature in forested habitats (McMahon et al. 2021). Ground area (i.e., the spatial area observed within each thermal picture) was added as an offset to the conditional model based on our a priori reasoning that a greater area observed would result in a greater probability of deer detection. Survey flight ID and survey year (0 = 2018, 1=2019) were included as crossed random intercepts to account for variation among survey flights and years.

We determined the proportion of cover types within each image by clipping land cover data (MN Land Cover Classification, 2013) with a 35-m buffer around the centroid of each thermal image using ArcMap 10.5.1 (Environmental Systems Research Institute, Inc., Redlands, CA, USA). The radius of 35 m was chosen so that the buffer area around each image centroid equaled the mean ground area captured in the thermal imagery. We calculated the ground area of the thermal imagery for each image from flight altitude data using the Pythagorean Theorem and then averaged across all images. Proportions of each land-cover class (developed, conifer forest, deciduous forest, forested wetland, emergent wetland, grassland, agriculture, and open water [i.e., snow-covered ice]) were considered individually and in meaningful groups: forested upland (conifer + deciduous), open upland (agriculture + grassland), wetland (forested wetland + emergent wetland), non-wetland open area (grassland + agriculture + developed + open water), and no cover (emergent wetlands + grass + water + agricultural + developed). The composite variables were chosen based on the type of resources they might provide in winter (e.g., food, cover) and whether a given vegetation type would likely be tall or dense enough to obscure a deer from aerial thermal detection.

Our deer detection data were saturated with ‘zero’ values so we implemented zero-inflated negative binomial and Poisson hurdle models in the glmmTMB package (Wenger and

Freeman 2008; Brooks et al. 2017). We modeled deer numbers separately for high (potential + certain deer detection counts) and low (certain deer detection counts) counts, using the same modeling approach for each set of counts. We ran all possible combinations of covariates and random effects in the conditional and binomial models for high and low deer counts. Candidate models were compared using Akaike's Information Criterion (AIC).

To predict the deer population size across the entirety of the CCESR property using our top-supported models of deer abundance (based on high and low count data), we created a virtual grid in Program R that covered the entire area. Each cell of the grid was 3,948 m^2 (62.83 m x 62.83 m), which equaled the mean ground area captured in the individual thermal images. We calculated the proportion of each land-cover type and composite cover-type variable within every grid cell using the land-cover data set and binning scheme described above. To generate a point estimate of the deer population size, we used the *predict* function in program R to estimate the probability of at least one deer being present (i.e., 1-P(structural zero)) and the expected mean of the conditional model for each grid cell (we assumed overcast sky conditions and random effects set to 0). The product of these two vectors (i.e., the expected number of deer per cell) was summed to provide an estimate of the deer population within the CCESR property.

To quantify uncertainty in our point estimate, we needed to account for uncertainty in our parameter estimates as well as stochasticity in the system. We first generated 10,000 sets of parameter values from a multivariate normal distribution with a mean vector set to the fitted coefficient values and a variance-covariance matrix extracted from the fitted model. These bootstrapped parameter values were then used to calculate expected probability of structural zeros and the conditional mean for each cell; random effects, if present in a given model, were generated from a normal distribution with mean = 0 and standard deviation extracted from the bootstrapped model parameters. We used these values to simulate our model for each grid cell by generating a sample from both the binomial and the conditional (either negative binomial or truncated Poisson) distributions and then calculating their product to yield a simulated number of deer within a given cell. These simulated deer numbers were summed across all cells to provide a simulated population estimate. This was repeated for each of the 10,000 sets of parameter values.

Pellet-group count surveys

We arranged pellet-group survey transects within the established UAS survey plots using a stratified random approach. We clipped land-cover data (MN Land Cover Classification, 2013) by the boundaries of the eight UAS survey plots and randomly inserted ~ 20 survey points proportionately with the availability of each cover type within the plot, using ArcMap. Our habitat cover types for conducting pellet-group counts included deciduous forest, forested wetland, emergent wetland, grass, and row crops. Transects were planned prior to fieldwork by using our stratified random points as starting locations and laying out a 100-m line in a direction from the starting point that would allow the surveyors to remain in the same habitat cover type for the entirety of the transect. Adjustments were made in the field as required to remain within the same habitat cover type.

Pellet-group counts were conducted during the months of April and May (2018 and 2019). We surveyed 133 transects in 2018 and resurveyed 120 of the same transects during 2019. Thirteen of the 2018 transects were not available for resurveying in 2019 due to prescribed burning on the CCESR property. Deer droppings were considered a pellet-group if there were at least 4 pellets of similar size, shape, and color within close proximity (pellets within 30 cm of each other). Pellet-groups were only counted if ≥50% of the pellet-group was within 1 m of the transect centerline, and they were determined to have been deposited after leaf-off the previous fall. Deciduous leaf litter falling between survey periods (2018 and 2019) eliminated the need to age or clear away pellet-groups, as only pellet-groups that had been deposited from fall to spring would be visible above the leaf litter. Where leaf litter was not present (e.g., open habitat types), we examined pellet-groups and determined deposition timing based on the presence of weather exposure, moss, and insect damage (Gable et al. 2017). Pellet-groups deposited post fall leaf-off would not likely show any such damage from exposure.

Pellet-group count data analysis and density modeling

We estimated deer density from pellet count data in two ways. In the first, we used a simple equation (Gable et al. 2017):

$$\textit{Deer density (deer/km}^2\textit{)} = \frac{pelletgroupscounted}{pelletgroupdepositionratexdepositionperiodxsamplingunitarea(km^2)}.$$

We considered the pellet deposition rate to be 25 pellet-groups/deer/day based on pellet count surveys from a study near International Falls, MN (Gable et al. 2017). This value is based on the mean values for deposition rate from two other studies; Rogers (1987) used a deposition rate of 34 and Patterson et al. (2002) used 16. We also calculated a low estimate using the value of 34 pellet-groups/deer/day and a high estimate using 16 pellet-groups/deer/day. Our pellet-group deposition period (time between mean leaf-off date and mean survey date) was 192 days for 2017–2018 and 209 days for 2018–2019. Density estimates were derived for forested (deciduous + forested wetland) and non-forested (emergent wetland + grass + row crops) habitat cover types by pooling count data from specific cover types for calculation, and averaging across survey years. Point estimates of deer density were predicted across CCESR by applying density estimates for forested and non-forested land cover to the proportion of forested and non-forested land cover of each grid cell in the virtual grid system described above in the *UAS Deer Density Modeling* section.

We also took a second approach, in which we fit a Poisson hurdle model to the number of pellet groups found per transect. We used the same potential covariates, random effects, and parametric bootstrapping approach that we used for the UAS models; we divided the total area of each land-cover type in the landscape into 200-m^2 transect units (i.e., equal in area to our sample transects). The result of predicting this model across each transect unit in the landscape was a "predicted number of pellets," that we converted to "predicted number of deer" by assuming a 192-day deposition period and the same high, low, and average pellet deposition rates used in the above equation.

Results

UAS-based deer density

We conducted either two or three replicate surveys over our eight UAS survey plots at CCESR during winter and spring of both 2018 and 2019, totaling 35 thermal UAS flights with analysable data. Our thermal surveys required a total of 24.7 hours of flight time with the PHX. We captured a total of 22,626 thermal images and analysed a subsample of 3,757 non-overlapping images. Of these images, 96.6% did not contain any potential deer detections. We classified 48 thermal images as containing certain deer detections (Fig. 2A) and an additional 95 with potential deer detections (Fig. 2B). Images with deer detections ranged in count from 1 to 9 individuals and we detected a total of 96 certain deer and an additional 135 potential deer within all survey images (Fig. 3). Our top performing model for high (i.e., certain + potential) deer detection was a zero-inflated negative binomial model that included the variables of sky cover ($\hat{\beta}$ = 3.14, SE = 0.45) and the proportion of wetland habitat cover ($\hat{\beta}$ = 0.66, SE = 0.21) in the conditional formula. The zero-inflated formula contained sky cover ($\hat{\beta}$ = 5.70, SE = 1.67) and the proportion of open upland habitat cover ($\hat{\beta}$ = 2.43, SE = 1.22; Table 1). Our top performing model for low (i.e., certain) deer detection was a truncated Poisson model that included sky cover ($\hat{\beta}$ = 0.90, SE = 0.43), the proportion of wetland habitat cover ($\hat{\beta}$ = 1.26, SE = 0.57), and a random effect for survey flight ID in the conditional formula, with the proportions of non-wetland open habitat cover ($\hat{\beta}$ = 3.46, SE = 1.26) in the zero-inflated formula (Table 1).

Our top detection models predicted mean point estimates for deer density of 12.38 and 6.18 deer/km^2 for the high and low detection estimates, respectively. Point abundance estimates were 273.81 deer and 136.68 deer on the CCESR property (22.12 km^2, Fig. 4, Table 2). Our bootstrapped estimates of deer density had a mean estimate of 13.77 deer/km^2 for the high detection model, and a mean of 9.40 deer for the low detection model. These density estimates equated to a mean of 304.55 deer on the CCESR property for the high-detection model, and 207.90 deer for the low-detection model (Fig. 4, Table 2).

Pellet-group count deer density

We surveyed 133 pellet-group count transects covering 26,600 m^2 in 2018 and recorded 1,085 pellet-groups. In 2019, we completed 120 transects equating to 24,000 m^2 surveyed, recording 766 pellet-groups.

Our predicted point estimates were 5.13, 6.98, and 10.91 deer/km^2 based on high (34 pellet groups/deer/day), mean (25 pellet groups/deer/day), and low (16 pellet groups/deer/day) deposition rates, respectively. Point estimates of abundance were 112.79 deer for high deposition, 153.39 deer for mean deposition, and 239.67 deer for low deposition on the CCESR property (Fig. 4, Table 2). The bootstrapped predictions resulted in a mean of 5.15 deer/km^2 for high deposition, a mean of 7.01 deer/km^2 for mean deposition, and a mean of 10.95 deer/km^2 for low deposition. The corresponding bootstrapped abundance estimates for CCESR from our bootstrapped prediction intervals were 113.25 deer, 154.02 deer, and 240.66 deer, respectively (Fig. 4, Table 2).

Overall, UAS and pellet-count survey-based methods yielded comparable results with overlapping estimates for CCESR. In particular, the bootstrapped abundance estimates from certain UAS detections and mean deposition rate pellet-group surveys had high overlap with a difference of 52.59 more deer estimated by UAS methodology. High (certain + potential) UAS detection estimates and pellet-group survey estimates based on low deposition rates also had large overlap with 61.34 more deer estimated by UAS over pellet-group surveys.

Discussion

We successfully applied UAS and FLIR technology to survey a wild population of white-tailed deer and compared the efficacy of this approach to pellet-group count surveys, a widely-used conventional method for surveying ungulate populations. Both of these methodologies yielded similar results for density and abundance estimates, dependent on the pellet model assumptions, yet varied in levels of sampling effort, cost, and time. Despite increasing use of UAS in wildlife research (Jiménez López and Mulero-Pázmány 2019), many studies rely on expensive UAS and sensors and do not assess how well the approach compares with established methods. However, understanding the logistical, financial and practical hurdles of incorporating UAS is especially important for wildlife managers with limited resources. Our findings provide insights into the process and utility of integrating UAS into monitoring ungulate populations in an efficient and temporally sensitive manner.

The most notable difference between pellet-group counts and UAS surveys was the amount of time and effort required for each approach. Pellet counts took approximately 160 hours (i.e., the time taken to count pellets and hike between survey transects) over both survey seasons, whereas the UAS surveys required only 24.7 hours of flight time in addition to approximately 30 minutes to one hour for set up and take down per launch site, totaling 17.5 to 35 hours of non-flight field effort. Time spent driving between UAS launch sites was negligible. An additional 25 to 35 hours of effort was required for manual review of thermal imagery. The physical effort required for pellet count surveys was greater, requiring large amounts of off-trail hiking to reach survey sites, relative to the majority of UAS launch sites off of drivable roads and trails. Pellet-group counts were also temporally restricted to just prior to spring green up, after all snow cover was melted, for maximum detectability of pellet-groups by human observers. Conversely, UAS FLIR surveys could be carried out with far greater flexibility and would have been feasible anytime from late November through April, at the northern latitude of our study site, which corresponded to leaf-off conditions for deciduous trees. Forest-dwelling ungulates can be successfully detected using FLIR-equipped UAS in leafless conditions (Witczuk et al 2018), and McMahon et al. (2021) found that increasing deciduous tree canopy hindered moose detection. The window of time for deciduous leaf-off conditions is relatively large at northern latitudes and is irrelevant for ungulate surveys in open grassland habitats. This wide temporal range allows researchers and managers greater operational flexibility for surveying ungulates, as compared to being seasonally restricted by pellet-group counts.

In addition to the temporal flexibility provided by the UAS approach, the added potential for frequently repeated surveys can provide managers with a means of rapidly conducting surveys to track how the space use and density of ungulate populations change through time. The ability to accurately, efficiently, and economically track ungulate population dynamics is paramount for management decisions because populations can change swiftly due to disease spread (Ditmer et al. 2020), interspecific competition (Weiskopf et al. 2019), changes in predator communities (Sivertsen et al. 2012), severe periods of weather (Bergman et al. 2015), and human land-use change (Fisher and Burton 2018). Barasona et al. (2014) utilised UAS imagery to model the environmental factors relating to the abundance of host species of tuberculosis in Spain (i.e., red deer [*Cervus elaphus*], fallow deer [*Dama dama*], and cattle [*Bos taurus*]). In Minnesota, chronic wasting disease is of special concern, where the movement of captive deer presents a risk for transmission to wild populations (Makau et al. 2020); applications of UAS similar to those used by Barasona et al. (2014) could provide important information regarding the presence and movement of wild deer in and around captive facilities. Moose populations have also experienced precipitous declines in northern Minnesota (DelGiudice 2018) and many traditional methods of population monitoring (e.g., capture and collaring) are currently restricted. McMahon et al. (2021) assessed the feasibility of monitoring this population's reproductive success without the need for traditional approaches that require handling of moose calves by using a FLIR-equipped UAS. The authors reported detecting GPS-collared adult moose with 85% success and non-collared moose calves with 79% success. They also were able to determine calf survival status after four separate suspected predation attempts, providing evidence that UAS can be used to monitor wild ungulate population demographics with less researcher-induced disturbance. However, McMahon et al. (2021) were only able to successfully gather data on individual wild moose fit with GPS collars and their calves; demonstrating the drawback of spatial limitations of UAS that prevent their application for extensive, large-scale wildlife surveys.

The application of UAS for surveying wild terrestrial species over spatially extensive areas has been largely impossible due to limitations of battery life, communication links, and federal regulations concerning commercial UAS use (Whitehead et al. 2014; Chrétien et al. 2016; Beaver et al. 2020). For example, Vincent et al. (2015) describes the regulation prohibiting the use of UAS beyond visual line of sight, and how this limits the ability to survey mobile wildlife over spatially extensive areas. Fixed-wing models of UAS currently offer the greatest solution for expanding UAS range, given their superior flight endurance over multi-copters (Linchant et al. 2015); however, the costs associated with our fixed-wing UAS (~$14,000) and thermal sensor (~ $3,200) do present a significant monetary barrier. Thermal sensors can be mounted on a less expensive quadcopter UAS, but times aloft (far slower flight speeds) and survey range for each flight become limited, with the additional prospect of disturbing the study species and non-target species due to quadcopters' much noisier operation (Scobie and Hugenholtz. 2016). We found another difficult tradeoff between multi-copter and fixed-wing UAS to be the extensive landing room required for fixed-wing operation. This is challenging in forested and semi-forested environments where sufficient landing zones are minimal. An additional major consideration for fixed-wing UAS operations is balancing UAS groundspeed (speed of UAS as measured in distance over the ground rather than through the air column) with FLIR sensor shutter speed. We recommend conducting test flights to ensure that images of the desired ground area can be captured with the required amount of image overlap prior to flying UAS for wildlife surveys. We experienced limitations of the amount of overlap we could obtain in our thermal images due to the relatively fast groundspeeds of the fixed-wing UAS; because our thermal sensor's shutter speed could not operate at speeds greater than 1.5 images/sec. We also experienced challenges with unreliable triggering of the thermal sensor during survey flights, which was addressed by debugging our novel pairing between FLIR and the PHX.

Accurately identifying deer from UAS-gathered thermal imagery was a challenge for estimating population abundance at CCESR. We collaborated with computer engineers to determine the feasibility of automating deer detection within our thermal imagery; however, this effort was unsuccessful due to the relatively low resolution of our imagery collected at flight altitudes of 121 m AGL. Automated detection algorithms are computationally complex (Chabot et al. 2018; Kellenberger et al. 2018), requiring either higher resolution sensors (which are substantially more expensive) or lower flight altitudes (which increase the risk of wildlife disturbance). These limitations may prevent wildlife managers and researchers from choosing to pursue automated detection, in favor of manual review (McMahon et al. 2021). However, manual review can be time consuming. Regardless of how detections are made, false positives and misidentification of species are prevalent issues in remote sensing applications (Brack et al. 2018; Kays et al. 2018). Conducting UAS surveys when thermal contrast between animal targets and their background environment is maximised (i.e., during early morning hours or overcast sky conditions which limit the amount of solar radiation that the ground absorbs) helps mitigate these issues and allows for greater thermal detection of target animals (Franke et al. 2012; Kays et al. 2018; Preston 2021). We modeled deer count data using both certain and potential detections as a sensitivity analysis to quantify how variability in detection influenced our population estimates. Including potential deer detections increased our mean population estimate, based on the bootstrapped prediction distribution, by 95 deer relative to the model only including certain detections (~46% increase). Potential deer detections may have included false positives (i.e., non-deer objects misidentified as deer) which would result in a higher abundance estimate, yet classifying only certain deer detections could have also mistaken actual deer for ground objects. As a post-hoc analysis we re-assessed 50% of the images that we initially considered to contain potential deer detections by examining the overlapping thermal imagery to quantify potential false negatives and positives. Our more thorough examination of each potential detection resulted in a 16% increase in certain detections and an 11% decrease in uncertain detections. This would result in a smaller difference between our certain and potential UAS deer estimates. While the additional effort would provide slightly more accurate population estimates, the approach is time consuming and may simply be unfeasible when considering larger areal coverage or more frequent flights. However, if researchers are able to overcome the previously mentioned hurdles to implementing accurate automated detection algorithms, the need to classify certainty and conduct the associated sensitivity analyses could be avoided.

Our estimates of deer abundance ended up being very similar despite the substantially different methodological approaches. This was especially true when comparing the prediction intervals for the pellet-group count model assuming 25 pellets/deer/day to the UAS model with certain deer only, and the pellet-group count model assuming a deposition rate of 16 pellets/day/deer to the more liberal certain + potential UAS model. Our findings highlight the sensitivity to the pellet deposition rate assumption previously described by Gable et al. (2017), and suggest that the highest deposition rate (34 pellets/deer/day) may be overestimated for our study area. Although the UAS models do not require quantifying a pellet deposition rate, a difficult value to validate, properly incorporating all aspects of uncertainty into our prediction intervals from the model structures used here was analytically complex. However, as the red-dashed lines in Figure 4 indicate, the simple mean point estimates from both pellet-group count and UAS models were similar to the bootstrapped mean prediction interval estimates from each model, suggesting that simple prediction methods may be sufficient if monitoring changes using an index of abundance is adequate (e.g., tracking monthly changes to density). Finally, while the upper tails of the distributions in our UAS model prediction intervals were extremely long, uncertainty could be reduced with more frequent surveys, surveying a greater extent of the study area, or any number of actions that reduced uncertainty in the detection process (e.g., flying lower and/or slower).

Technological advances, along with new tools and methodologies are increasingly available for wildlife managers, yet few studies consider all of the practical aspects of their field use or how they compare with established methods. Pellet-group counts and other ground-based methodologies are relatively affordable, well-understood and documented in the literature, and require less training than novel technological approaches. However, following an initial financial investment and training period, UAS allows for rapid survey capabilities over areas of rough terrain with few restrictions on time and available human effort that control many other methods. Continued advancement and reduction of costs for UAS, FLIR, and automated image analysis technology will likely continue to expand the applications of UAS in wildlife population surveys, making UAS a more readily applicable tool for wildlife managers to include in their toolbox. Tools that can improve the frequency of data collection and accuracy of population monitoring will be even more essential in the coming decades where wildlife must adapt to numerous environmental changes.

Conflicts of interest

There are no conflicts of interest to report.

Acknowledgements

We thank Dr. F. Isbell, Dr. C. Potter, T. Mielke, and the rest of the staff at the Cedar Creek Ecosystem Science Reserve for their assistance with project planning and field support. We thank Dr. T. Arnold and Dr. J. Knight of the University of Minnesota Twin Cities for their advisement and input. We thank T. Colten and M. Skelton of Sentera for their technical support and field assistance with deploying the PHX. We thank J. Tillery and D. Brown for their assistance as field technicians. Funding was provided by the Minnesota Agricultural Experiment Station (Project# MIN-41-020), the University of Minnesota Graduate School (fellowship support for M. McMahon), and the Environment and Natural Resources Trust Fund as recommended by the Legislative-Citizen Commission on Minnesota Resources.
We also recognise the University of Minnesota Department of Fisheries, Wildlife, and Conservation Biology for its technical support on this project.

References

Allan, B. M., Nimmo, D. G., Ierodiaconou, D., VanDerWal, J., Koh, L. P., and Ritchie, E.G. (2018). Futurecasting ecological research: the rise of technology. *Ecosphere* **9**(5), e02163.

Barasona, J. A., Mulero-Pázmány, M., Acevedo, P., Negro, J. J., Torres, M. J., Gortázar, C., and Vicente, J. (2014). Unmanned aircraft systems for studying spatial abundance of ungulates: relevance to spatial epidemiology. *PLoS ONE* **9**(12), e115608.

Beaver, J. T., Baldwin, R. W., Messinger, M., Newbolt, C. H., Ditchkoff, S. S., and Silman, M. R. (2020). Evaluating the use of drones equipped with thermal sensors as an effective method for estimating wildlife. *Wildlife Society Bulletin* **44,** 434-443.

Bennett, L. J., English, P. F., and McCain, R. (1940). A study of deer populations by use of pellet-group counts. *The Journal of Wildlife Management* **4**(4), 398-403.

Bennitt, E., Bartlam-Brooks, H. L. A., Hubel, T. Y., and Wilson, A. M. (2019). Terrestrial mammalian wildlife responses to Unmanned Aerial Systems approaches. *Scientific Reports* **9**, 2142.

Bergman, E. J., Doherty, P. F., White, G. C., and Holland, A. A. (2015). Density dependence in mule deer: a review of evidence. *Wildlife Biology* **21**, 18-29.

Bonenfant, C., Pelletier, F., Garel, M., and Bergeron, P. (2009). Age-dependent relationship between horn growth and survival in wild sheep. *Journal of Animal Ecology* **78**, 161-171.

Brack, I. V., Kindel, A., and Oliveira, L. F. B. (2018). Detection errors in wildlife abundance estimates from unmanned aerial systems (UAS) surveys: synthesis, solutions, and challenges. *Methods in Ecology and Evolution* **9**, 1864-1873.

Brinkman, T. J., Jenks, J. A., DePerno, C. S., Haroldson, B. S., and Osborn, R. G. (2004). Survival of white-tailed deer in an intensively farmed region of Minnesota. *Wildlife Society Bulletin* **32**(3), 726-731.

Brooks M. E., Kristensen, K., van Benthem, K. J., Magnusson, A., Berg, C. W., Nielsen, A., Skaug, H. J., Maechler, M., and Bolker, B. M. (2017). glmmTMB Balances speed and flexibility among packages for zero-inflated generalized linear mixed modeling. *The R Journal* **9**(2), 378-400.

Cedar Creek Ecosystem Science Reserve. (2019). History Summary. <www.cedarcreek.umn.edu/about/history>. Accessed 19 Nov 2019.

Chabot, D., Dillon, C., and Francis, C. M. (2018). An approach for using off-the-shelf object-based image analysis software to detect and count birds in large volumes of aerial imagery. *Avian Conservation and Ecology* **13**(1), 15.

Chabot, D., and Bird, D. M. (2012). Evaluation of an off-the-shelf unmanned aircraft system for surveying flocks of geese. *Waterbirds* **35**, 170-174.

Chrétien, L.-P., Théau, J., and Ménard, P. (2016). Visible and thermal infrared remote sensing for the detection of white-tailed deer using an unmanned aerial system. *Wildlife Society Bulletin* **40**, 181-191.

Dawe, K. L., and Boutin, S. (2016). Climate change is the primary driver of white-tailed deer (Odocoileus virginianus) range expansion at the northern extent of its range; land use is secondary. *Ecology and Evolution* **6**, 6435-6451.

Del Giudice, G. D. (2018). 2018 Aerial moose survey. Minnesota Department of Natural Resources, Forest Wildlife Populations and Research Group. Grand Rapids, Minnesota, USA.

Ditmer, M. A., McGraw, A. M., Cornicelli, L., Forester, J. D., Mahoney, P. J., Moen, R. A., Stapleton, S. P., St-Louis, V., VanderWaal, K., and Carstensen, M. (2020). Using movement ecology to investigate meningeal worm risk in moose, Alces alces. *Journal of Mammalogy* **101**, 589-603.

Dunn, W. C., Donnelly, J. P., and Krausmann, W. J. (2002). Using thermal infrared sensing to count elk in the southwestern United States. *Wildlife Society Bulletin* **30**(3), 963-967.

Eberhardt, L., and Van Etten, R. C. (1956). Evaluation of the pellet group count as a deer census method. *The Journal of Wildlife Management* **20**(1), 70-74.

Edmunds, D. R., Kauffman, M. J., Schumaker, B. A., Lindzey, F. G., Cook, W. E., Kreeger, T. J., Grogan, R. G., and Cornish, T. E. (2016). Chronic wasting disease drives population decline of white-tailed deer. *PLoS ONE* **11**(8), e0161127.

Elsey, R. M., and Trosclair, P. L. III., (2016). The use of an unmanned aerial vehicle to locate alligator nests. *Southeastern Naturalist* **15**(1), 76-82.

Fisher, J. T., and Burton, A. C. (2018). Wildlife winners and losers in an oil sands landscape. *Frontiers in Ecology and the Environment* **16**, 323-328.

Franke, U., Goll, B., Hohmann, U., and Heurich, M. (2012). Aerial ungulate surveys with a combination of infrared and high-resolution natural colour images. *Animal Biodiversity and Conservation* **35.2**, 285-293.

Gable, T. D., Windels, S. K., and Olson, B. T. (2017). Estimates of white-tailed deer density in Voyageurs National Park: 1989–2016. Natural Resource Report NPS/VOYA/NRR—2017/1427. National Park Service, Fort Collins, Colorado.

Gesch, D., Oimoen, M., Greenlee, S., Nelson, C., Steuck, M. and Tyler, D., (2002). The national elevation dataset. *Photogrammetric Engineering and Remote Sensing*. **68**(1), 5-32.

Gill, R. M. A., Thomas, M. L., and Stocker, D. (1997). The use of portable thermal imaging for estimating deer population density in forest habitats. *Journal of Applied Ecology* **34**, 1273-1286.

Grovenburg, T. W., Swanson, C. C., Jacques, C. N., Klaver, R. W., Brinkman, T. J., Burris, B. M., DePerno, C. S., and Jenks, J. A. (2011). Survival of white-tailed deer neonates in Minnesota and South Dakota. *Journal of Wildlife Management* **75**(1), 213-220.

Hodgson, J. C., and Koh, L. P. (2016). Best practice for minimising unmanned aerial vehicle disturbance to wildlife in biological field research. *Current Biology* **26**, 404-405.

Hodgson, J. C., Mott, R., Baylis, S. M., Pham, T. T., Wotherspoon, S., Kilpatrick, A. D., Raja Segaran, R., Reid, I., Terauds, A., and Koh, L. P. (2018). Drones count wildlife more accurately and precisely than humans. *Methods in Ecology and Evolution* **2018**, 1-8.

Ireland, A. W., Palandro, D. A., Garas, V. Y., Woods, R. W., Davi, R. A., Butler, J. D., Gibbens, D. M., and Gibbens, J. S. (2019). Testing unmanned aerial systems for monitoring wildlife at night. *Wildlife Society Bulletin* **43**, 182-190.

Israel, M. (2011). A UAV-based roe deer fawn detection system. *International Archives of the Photogrammetry, Remote Sensing and Spatial Information Sciences* **38**, 51-55.

Jennelle, C. S., Henaux, V., Wasserberg, G., Thiagarajan, B., Rolley, R. E, and Samuel, M. D. (2014). Transmission of chronic wasting disease in Wisconsin white-tailed deer: Implications for disease spread and management. *PLoS ONE* **9**, e91043.

Jiménez López, J., and Mulero-Pázmány, M. (2019). Drones for conservation in protected areas: present and future. *Drones* **3**, 1-23.

Kays, R., Sheppard, J., Mclean, K., Welch, C., Paunescu, C., Wang, V., Kravit, G., and Crofoot, M. (2018). Hot monkey, cold reality: surveying rainforest canopy mammals using drone-mounted thermal infrared sensors. *International Journal of Remote Sensing* **40**(2), 4070-419.

Kellenberger, B., Marcos, D., and Tuia, D. (2018). Detecting mammals in UAV images: best practices to address a substantially imbalanced dataset with deep learning. *Remote sensing of Environment* **216**, 139-153.

Krause, D. J., Hinke, J. T., Perryman, W. L., Goebel, M. E., and LeRoi, D. J. (2017). An accurate and adaptable photogrammetric approach for estimating the mass and body condition of pinnipeds using and unmanned aerial system. *PLoS ONE* **12**(11), e0187465.

Lethbridge, M., Stead, M., and Wells, C. (2019). Estimating kangaroo density by aerial survey: a comparison of thermal cameras with human observers. *Wildlife Research* **46**, 639-648.

Lhoest, S., Linchant, J., Quevauvillers, S., Vermeulen, C., and Lejeune, P. (2015). How many hippos: algorithm for automatic counts of animals with infra-red thermal imagery from UAV. *International Archives of the Photogrammetry, Remote Sensing and Spatial Information Sciences* **40**, 355-362.

Linchant, J., Tech, G. A., and Management, F. R. (2015). Are unmanned aircraft systems (UASs) the future of wildlife monitoring? A review of accomplishments and challenges. *Mammal Review* **45**, 239-252.

Makau, D. N., Vanderwaal, K., Kincheloe, J. and Wells, S. J. (2020). Implications of farmed-cervid movements on the transmission of chronic wasting disease. *Preventative Veterinary Medicine* **182**, 105088.

McMahon, M. C., Ditmer, M. A., Isaac, E. J., Moore, S. A., and Forester, J. D. (2021). Evaluating unmanned aerial systems for the detection and monitoring of moose in northeastern Minnesota. *Wildlife Society* Bulletin **DOI: 10.1002/wsb.1167**, 1-13.

Mech, L. D., Fieberg, J., and Barber-Meyer, S. (2018). An historical overview and update of wolf-moose interactions in northeastern Minnesota. *Wildlife Society Bulletin* **42**(1), 40-47.

Minnesota Department of Natural Resources [MNDNR]. (2019). Climate of Minnesota. <www.dnr.state.mn.us/climate/historical/acis_stn_meta.html>. Accessed 18 Nov 2019.

Mulero-Pázmány, M., Jenni-Eiermann, S., Strebel, N., Sattler, T., Negro, J. J., and Tablado, Z., (2017). Unmanned aircraft systems as a new source of disturbance for wildlife: a systematic review. *PLoS ONE* **12**, 1-17.

Mulero-Pázmány, M., Stolper, R., van Essen, L. D., Negro, J. J., and Sassen, T. (2014). Remotely Piloted Aircraft Systems as a Rhinoceros Anti-Poaching Tool in Africa. *PLoS ONE* **9**.

Mysterud, A. (2006). The concept of overgrazing and its role in management of large herbivores. *Wildlife Biology* **12**, 129-141.

National Land Cover Database 2011 (NLCD 2011). Multi-Resolution Land Characteristics Consortium (MRLC). https://data.nal.usda.gov/dataset/national-land-cover-database-2011-nlcd-2011.

Naugle, D. E., Jenks, J. A., and Kernoham, B. J. (1996). Use of thermal infrared sensing to estimate density of white-tailed deer. *Wildlife Society Bulletin* **24**(1), 37-43.

Patterson, B. R., Macdonald, B. A., Lock, B. A., Anderson, D. G., and Benjamin, L. K. (2002). Proximate factors limiting population growth of white-tailed deer in Nova Scotia. *Journal of Wildlife Management* **66**, 511-521.

Plante, S., Dussault, C., Richard, J. H., and Côte, S. D. (2018). Human disturbance effects and cumulative habitat loss in endangered migratory caribou. *Biological Conservation* **224**, 129-143.

Preston, T. M., Wildhaber, M. L., Green, N. S., Albers, J. L., and Debenedetto, G. P. (2021). Enumerating white-tailed deer using unmanned aerial vehicles. *Wildlife Society Bulletin* **45**(1), 97-108.

Rampi, L. P., Knight, J. F., Bauer, M. (2016). Minnesota land cover classification and impervious surface area by Landsat and Lidar: 2013 Update. Retrieved from the Data Repository for the University of Minnesota, http://doi.org/10.13020/D6JP4S.

Rhoads, C. L., Bowman, J. L., and Eyler, B. (2010). Home range and movement rates of female exurban white-tailed deer. *Journal of Wildlife Management* **74**(5), 987-994.

Rogers, L. L. (1987). Seasonal changes in defecation rates of free-ranging white-tailed deer. *The Journal of Wildlife Management* **51**(2), 330-333.

Sasse, D. B. (2003). Job-related mortality of wildlife workers in the United States, 1937-2000. *Wildlife Society Bulletin* **31**, 1015-1020.

Scobie, C. A., and Hugenholtz, C. H. (2016). Wildlife monitoring with unmanned aerial vehicles: Quantifying distance to auditory detection. *Wildlife Society Bulletin* **40**, 781-785.

Siversten, T. R., Mysterud, A. and Gundersen, H. (2012). Moose (Alces alces) calf survival in the presence of wolves (Canis lupus) in southeast Norway. European *Journal of Wildlife Research* **58**, 863-868.

Vermeulen, C., Lejeune, P., Lisein, J., Sawadogo, P., Bouché, P. (2013). Unmanned aerial survey of elephants. *PLoS ONE* **8**(2), e54700.

Vincent, J. B., Werden, L. K., and Ditmer, M. A. (2015). Barriers to adding UAVs to the ecologist's toolbox. *Ecological Society of America* **13**, 74-75.

Wallmo, O. C., Jackson, A. W., Hailey, T. L., Carlisle, R. L. (1962). Influence of rain on the count of deer pellet groups. *The Journal of Wildlife Management* **26**(1), 50-55.

Watts, A. C., Perry, J. H., Smith, S. E., Burgess, M. A., Wilkinson, B. E., Szantoi, Z., Ifju, P. G., and Percival, H. F. (2010). Small unmanned aircraft systems for low-altitude aerial surveys. *Journal of Wildlife Management* **74**, 1614-1619.

Weiskopf, S. R., Ledee, O. E., and Thompson, L. M. (2019). Climate change effects on deer and moose in the Midwest. *The Journal of Wildlife Management* **83**(4), 769-781.

Weissensteiner, M. H., Poelstra, J. W., and Wolf, J. B. W. (2015). Low-budget ready-to-fly unmanned aerial vehicles: an effective tool for evaluating the nesting status of canopy-breeding bird species. *Journal of Avian Biology* **46**, 425-430.

Werden, L. K., Vincent, J. B., Tanner, J. C., and Ditmer, M. A. (2015). Not quite free yet: clarifying UAV regulatory progress for ecologists. *Frontiers in Ecology and the Environment* **13**(10), 534-535.

Whitehead, K., Hugenholtz, C. H., Myshak, S., Brown, O., Leclair, A., Tamminga, A., Barchyn, T. E., Moorman, B., and Eaton, B. (2014). Remote sensing of the environment with small unmanned aircraft systems (UASs), part 2: scientific and commercial applications. *Journal of Unmanned Vehicle Systems* **2**, 86-102.

Witczuk, J., Pagacz, S., Zmarz, A., and Cypel, M. (2018). Exploring the feasibility of unmanned aerial vehicles and thermal imaging for ungulate surveys in forests - preliminary results. *International Journal of Remote Sensing* **39**, 5504-5521.

Figures and tables

Figure 1: Cedar Creek Ecosystem Science Reserve (CCESR) study area, Minnesota, USA. Unmanned aerial system (UAS) survey plots are distinguished by the teal, numbered boundaries. Plot 8 was omitted from our study because of our inability to safely land the UAS at that site.

Figure 2: Thermal imagery of certain white-tailed deer (*Odocoileus virginianus*) detections (A) and potential deer detections (B) collected at Cedar Creek Ecosystem Science Reserve,

Minnesota, USA during UAS surveys from March to April of 2018 and from January to March of 2019. We distinguished between certain and potential deer detections by shape, brightness, and size of thermal signatures. Figure 2A shows clear thermal signatures of deer based on these factors, while figure 2B contains less certainty based on shape. Such signatures were still counted as potential deer because shape can vary greatly in thermal imagery (e.g., when deer are bedded down versus standing/walking).

Figure 3: Histogram showing the number of UAS images with 1–9 certain or potential white-tailed deer (*Odocoileus virginianus*) detections from thermal imagery during unmanned aerial system surveys at the Cedar Creek Ecosystem Science Reserve, Minnesota, USA from March to April of 2018 and from January to March of 2019. Overall, deer counts per image ranged from 1 to 9 deer, with 3,631 images containing no detection. We distinguished between certain and potential deer detections by shape, brightness, and size of thermal signatures.

Figure 4: Boxplots of the bootstrapped predictions of the number of estimated deer in the Cedar Creek Ecosystem Science Reserve, Minnesota, USA based on pellet-group count models assuming high, mean, and low rates of pellet deposition (34, 25 & 16 pellets per deer per day, respectively) and UAS models using counts of certain and certain plus potential white-tailed deer in thermal images. Surveys were conducted from March to May of 2018 and from January to May of 2019. Orange points represent the means of the bootstrapped predictions. Red-dashed lines on each pellet-based model show the model-free point estimates. The red dashed-lines over the UAS model estimates represent mean point estimates from the top model for certain and certain plus potential deer detections.

Figure 1

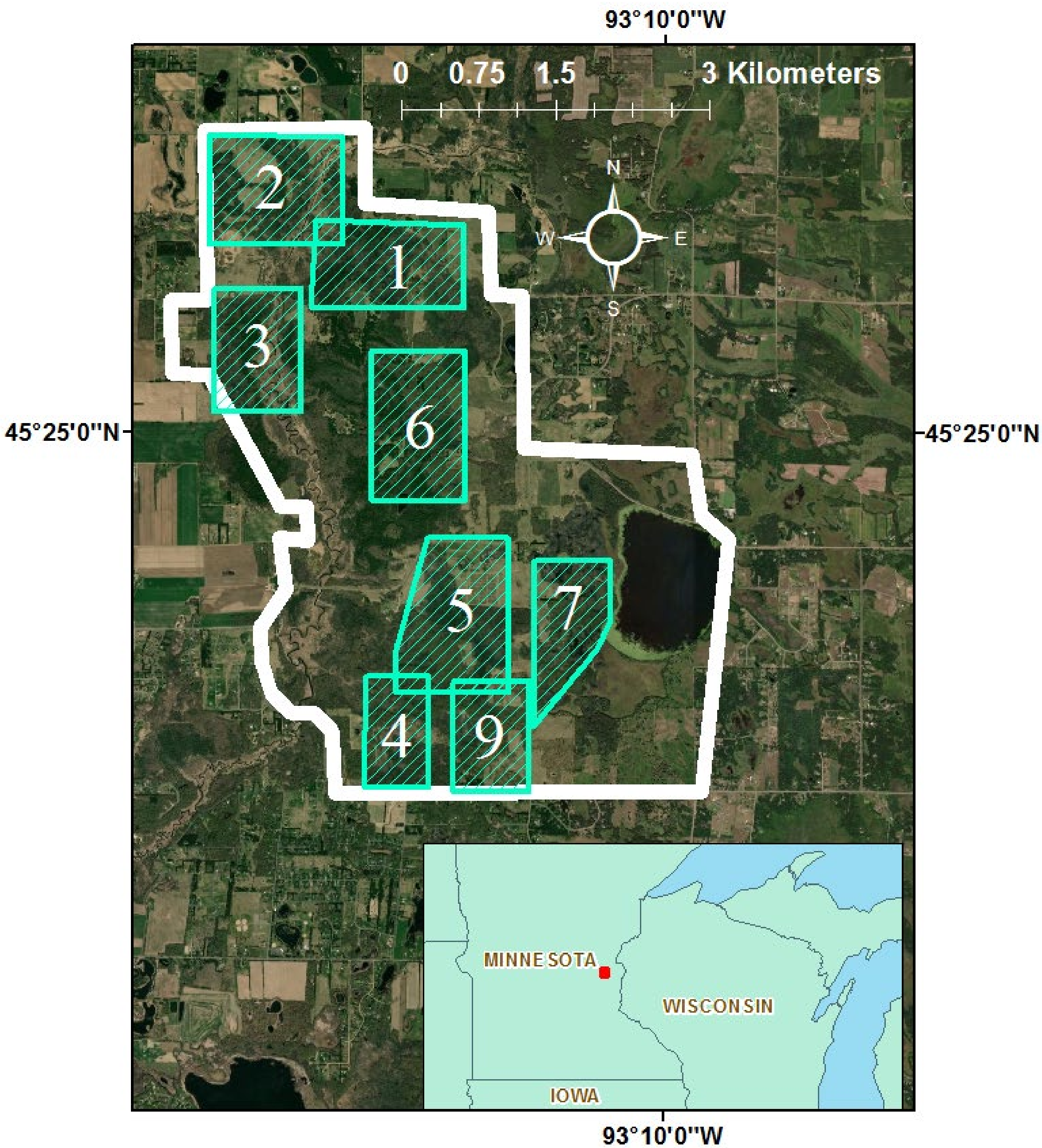
93°10'0"W
0
0.75
1.5
3 Kilometers
N
W
E
S
2
1
3
6
5
7
4
9
45°25'0"N
45°25'0"N
MINNESOTA
WISCONSIN
IOWA
93°10'0"W

Figure 2

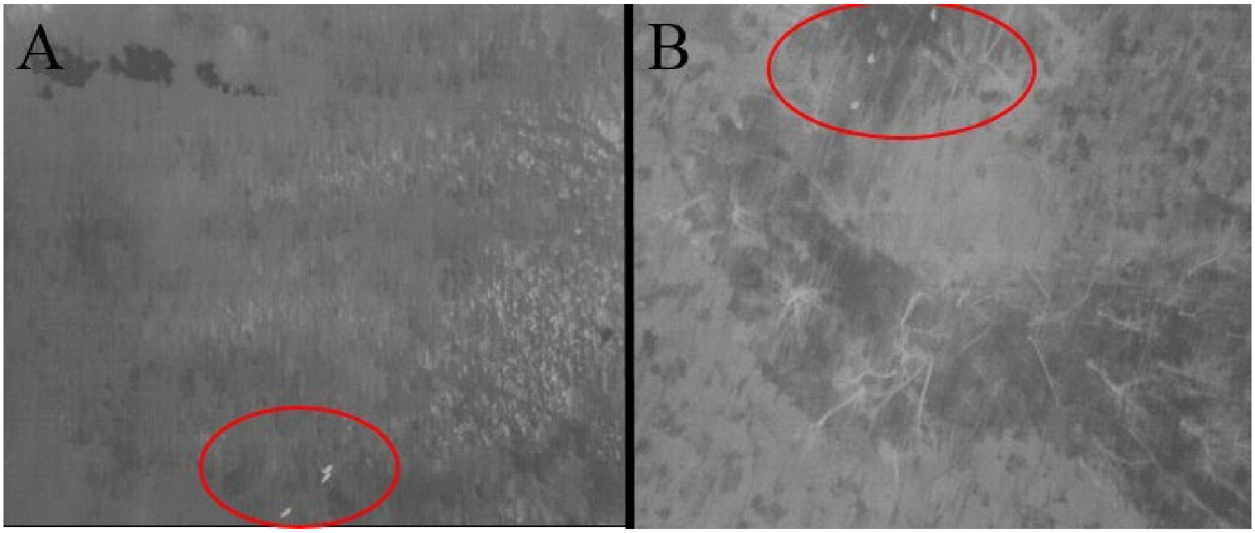

Figure 3

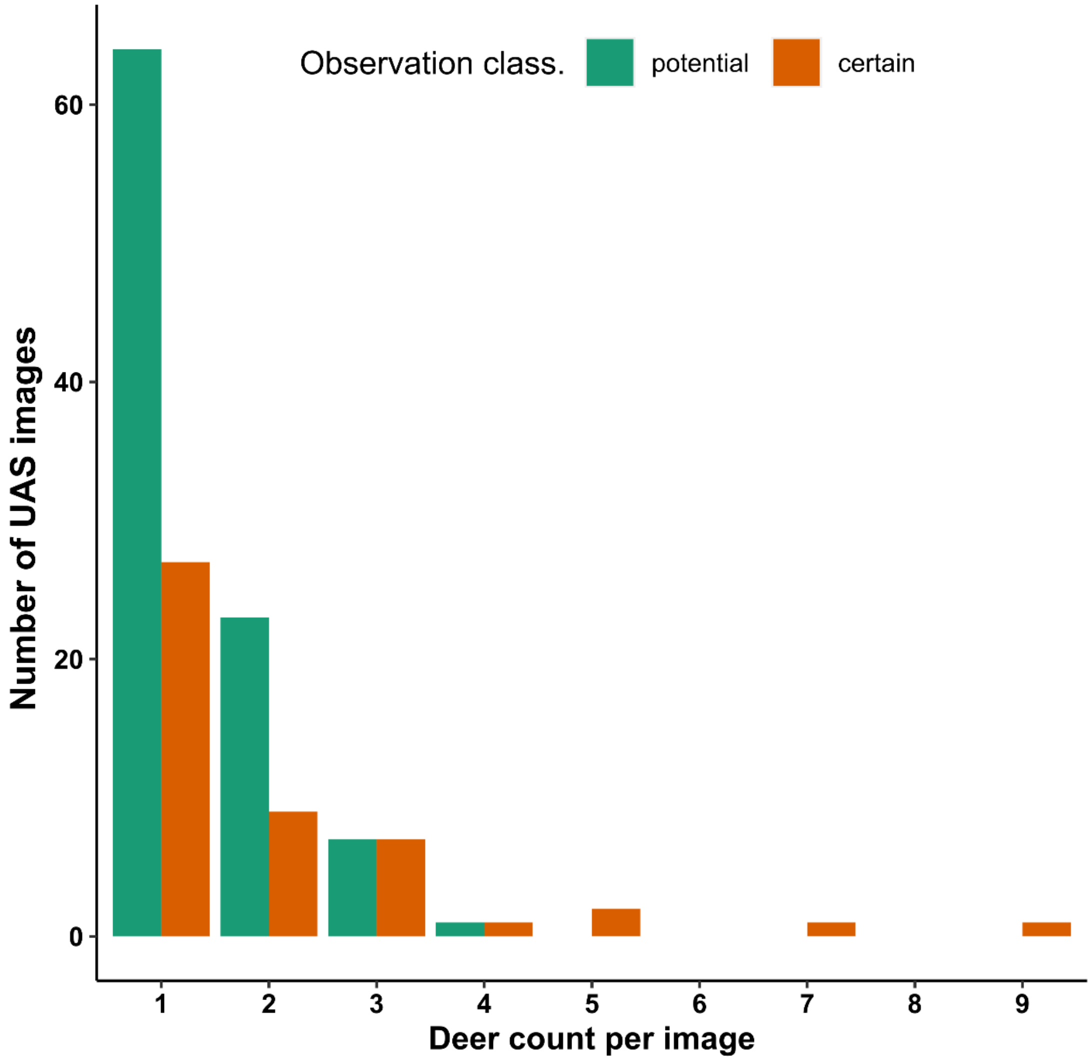
Observation class.
potential
certain
Number of UAS images
0
20
40
60
1
2
3
4
5
6
7
8
9
Deer count per image

Figure 4

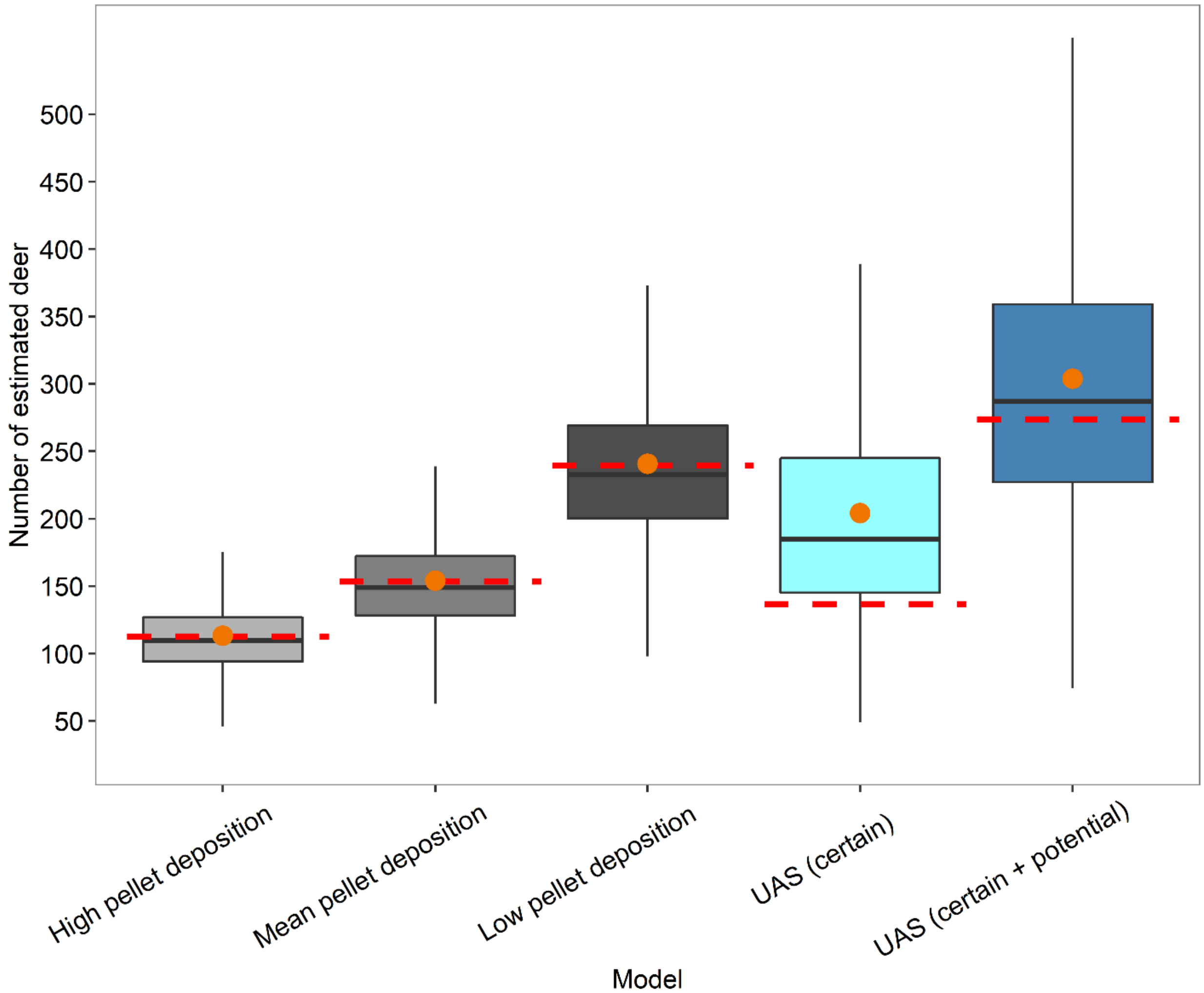
500
450
400
350
300
250
200
150
100
50
Number of estimated deer
High pellet deposition
Mean pellet deposition
Low pellet deposition
UAS (certain)
UAS (certain + potential)
Model

Table 1: The highest-ranking models for estimating deer abundance based on detection data from unmanned aerial system surveys from March to April of 2018 and from January to March of 2019 at Cedar Creek Ecosystem Science Reserve, Minnesota, USA. We estimated deer abundance based on high (certain + potential) deer detections (Response Type = High) and low (certain) deer detections (Response Type = Low). We considered various distributions (*Family*) for modeling deer abundance, but show only the top performing distributions for each response type. All models included an offset for ground area captured in the analysed thermal image. Model ranking (*Rank*) is based on ΔAIC.

Formula	Family	loglik	ΔAIC	Rank
Response Type = High				
Conditional Formula = ~Sky Cover + Proportion Wetland*, Zero-Inflated Formula = ~Sky Cover + Proportion Open Upland**	Zero-inflated Negative Binomial	-694.9	0	1
Conditional Formula = ~Sky Cover + Proportion Wetland + Random Effect for Survey Flight ID, Zero-Inflated Formula = ~Sky Cover + Proportion Open Upland	Zero-inflated Negative Binomial	-694.7	1.7	2
Conditional Formula = ~Sky Cover + Proportion Wetland + Random Effect for Survey Year, Zero-Inflated Formula = ~Sky Cover + Proportion Open Upland	Zero-inflated Negative Binomial	-694.9	2	3
Response Type = Low				
Conditional Formula = ~ Sky Cover + Proportion Wetland + Random Effect for Survey Flight ID, Zero-Inflated Formula = ~ Proportion Non-Wetland Open***	Truncated Poisson	-306.9	0	1

Conditional Formula = ~ Sky Cover + Proportion Wetland, Zero-Inflated Formula = ~ Proportion Non-Wetland Open	Truncated Poisson	-308.7	1.6	2
Conditional Formula = ~ Sky Cover + Proportion Conifer + Proportion Deciduous, Zero-Inflated Formula = ~ Proportion Non-Wetland Open	Truncated Poisson	-309.2	2.6	3

*Wetland habitat is defined as forested wetland + emergent wetland habitats

**Open upland habitat is defined as row crops (agricultural) + grass habitats

***Non-wetland open habitat is defined as row crops (agricultural) + grass + developed + open water habitats

Table 2: White-tailed deer density and abundance estimates from unmanned aerial system (UAS) surveys and pellet-group counts from March to May of 2018 and from January to May of 2019 at the Cedar Creek Ecosystem Science Reserve (CCESR), Minnesota, USA. UAS high estimates are based on certain + potential thermal detections, and UAS low detections are based on only certain detections. Pellet estimates are from pellet-group surveys with low estimates corresponding to 34 pellet groups per deer per day, mean estimates to 25 pellet groups per deer per day, and high estimates to 16 pellet groups per deer per day. Point estimates do not include estimates of error. 95% prediction intervals were calculated through bootstrapped estimates.

	CCESR Density (deer/km2)	**95% Prediction Interval (deer/km2)**	**CCESR (total deer)**	**95% Prediction Interval (total deer)**
UAS High Point Estimate	12.38	-	273.81	-
UAS Low Point Estimate	6.18	-	136.68	-

UAS High Bootstrapped Estimate	13.77	6.64-24.35	304.55	146.88-538.62
UAS Low Bootstrapped Estimate	9.40	4.32-17.84	207.90	95.56-394.62
Pellet Low Point Estimate	5.13	-	112.79	-
Pellet Mean Point Estimate	6.98	-	153.39	-
Pellet High Point Estimate	10.91	-	239.67	-
Pellet Low Bootstrapped Estimate	5.15	3.04-8.30	113.25	66.82-182.48
Pellet Mean Bootstrapped Estimate	7.01	4.14-11.29	154.02	90.88-248.18
Pellet High Bootstrapped Estimate	10.95	6.46-17.65	240.66	142.00-387.78